Research Square

Preprints are preliminary reports that have not undergone peer review.
They should not be considered conclusive, used to inform clinical practice,
or referenced by the media as validated information.

Viscoelastic characterization of 100% RAP from different sources using the impact resonance test: repeatability, reproducibility, and effect of compaction temperature

Thamires Ximenes Cavalcante

thamires.ximenes-cavalcante.2@ens.etsmtl.ca

École de Technologie Supérieure

Jean-Claude Carret

École de Technologie Supérieure

Kevin Bilodeau

Bauval Inc

Lucas F. de A. L. Babadopulos

Universidade Federal do Ceará

Research Article

Keywords: Impact Resonance Test, Reclaimed Asphalt Pavement, Complex Modulus, Phase Angle, Compaction Temperature, Air Voids

Posted Date: November 25th, 2026

DOI: https://doi.org/10.21203/rs.3.rs-11392505/v1

License: This work is licensed under a Creative Commons Attribution 4.0 International License.
Read Full License

Additional Declarations: No competing interests reported.

Viscoelastic characterization of 100% RAP from different sources using the impact resonance test: repeatability, reproducibility, and effect of compaction temperature

Thamires Ximenes Cavalcante[1*], Jean-Claude Carret[1], Kevin Bilodeau[2] and Lucas F. de A. L. Babadopulos[3].

[1]École de technologie supérieure, Montréal, Québec, Canada
[2]Bauval Inc., Boucherville, Québec, Canada
[3]Universidade Federal do Ceará, Fortaleza, Brasil

*Corresponding author(s). E-mail(s): thamires.ximenes-cavalcante.2@ens.etsmtl.ca;
Contributing authors: Jean-Claude.Carret@etsmtl.ca; kbilodeau@bauval.com; babadopulos@ufc.br

Abstract

This study proposes a methodology based on mechanical wave propagation (MWP), utilizing the impact resonance test (IRT), to characterize and compare the viscoelastic response of reclaimed asphalt pavement (RAP) compacted at different temperatures and with varying void contents. The IRT allows determining the norm of complex modulus ($|E^*|$) and its phase angle (φ) from the resonance response of specimens. Tests were conducted on mixtures composed only of RAP (100% RAP), compacted at different temperatures (110, 130, 150, and 170 °C) and tested across a range of temperatures (from -30 °C to 40 °C). The repeatability of the IRT results was evaluated based on five impacts per test in both a university laboratory and an industry laboratory, while reproducibility was analyzed by comparing measurements obtained independently at the two laboratories. The results indicated low variability between impacts and good reproducibility between laboratories, highlighting the potential of the proposed methodology in both academic research and industrial practice. Furthermore, it was observed that $|E^*|$ was influenced by both compaction temperature and void content, whereas no clear relationship was observed between φ and void content. The variation of φ as a function of compaction temperature proved to be a potential indicator for differentiating RAP sources based on their response to compaction temperature. The proposed methodology demonstrates potential for the non-destructive characterization and differentiation of the viscoelastic response of recycled asphalt mixtures.

Keywords: Impact Resonance Test, Reclaimed Asphalt Pavement, Complex Modulus, Phase Angle, Compaction Temperature, Air Voids.

1 Introduction

Amid the growing demand for sustainable solutions in pavement engineering, reclaimed asphalt pavement (RAP) has emerged as an important material for supporting more

sustainable practices by enabling the reuse of existing asphalt materials and reducing the demand for virgin aggregates and bitumen [1-3]. Consequently, several studies have investigated the characterization and potential applications of RAP at various percentages in asphalt mixtures (AM) [4-13]. However, the use of RAP in AM requires the consideration of multiple factors, since its properties can vary significantly depending on composition, origin, service history, and the degree of binder aging.

Considering these aspects, characterizing the mechanical response of RAP prior to its incorporation into new mixtures is of great relevance. However, conventional approaches for characterizing RAP binder properties generally involve binder extraction and recovery, followed by mechanical or rheological testing of the binder phase. However, these procedures can be costly and time-consuming, and they require chemical solvents that may affect the properties of the recovered binder [14, 15]. Moreover, the procedure could potentially lead to different results than testing the RAP directly.

In this context, non-destructive testing (NDT) methods, such as the impact resonance test (IRT), serve as alternative approaches for characterizing the viscoelastic response of RAP without binder extraction. The IRT enables the determination of viscoelastic parameters in AM, such as the norm of complex modulus ($|E^*|$) and phase angle (φ), in a practical and reproducible way [16-24]. It also provides a quick, economical, and easy approach compared to traditional methods.

Given its potential, as well as that of other NDT methods based on mechanical wave propagation, the RILEM Technical Committee 331-MWP: Mechanical Wave Propagation to Characterize Bituminous Mixtures was established in fall 2024. The committee's main objective is to provide guidelines for performing and analyzing ultrasonic and impact resonance methods to assess the LVE properties of AM [16].

According to the TC 331-MWP introductory letter, one of the main challenges in applying MWP-based methods to viscoelastic materials, such as AM, is the lack of standardized testing procedures and guidelines for interpreting the results [16]. In this context, this study proposes a methodology based on MWP using IRT to characterize and distinguish the viscoelastic response of different sources of 100% RAP. Specifically, the study aims to: (i) evaluate the repeatability of IRT measurements and the reproducibility between a university laboratory and an industry laboratory; (ii) investigate the effects of compaction temperature and air void content on $|E^*|$ and φ; and (iii) explore the potential of viscoelastic parameters obtained via IRT to distinguish between different RAP sources.

2 Materials and Methods

2.1 Materials

In this study, three materials composed of 100% RAP, named RAP A, B, and C, were evaluated. For each type of RAP, four specimens were produced at different compaction temperatures (110, 130, 150, or 170°C) to evaluate the impact of the compaction temperature on the mechanical properties of the RAP specimens. The compaction temperature range from 110°C to 170°C was selected to cover conditions from relatively low compaction temperatures, allowing for sufficient binder workability and adhesion to aggregates during compaction, to higher compaction temperatures approaching the upper heated limits commonly used in the AM production process. Compaction was performed with a shear gyratory compactor, using 200 gyrations, and the specimens were subsequently cut with a

concrete saw to obtain disk-shaped specimens. Table 1 shows the physical and geometrical properties of the specimens. The air void content (V_a) was estimated based on the dry mass and apparent volume.

Table 1. Physical and geometrical properties of specimens.

Material	Compaction Temperature (°C)	Diameter (mm)	Height (mm)	Mass (g)	G_{mm}	V_a(%)
RAP A	110	149.8	56.7	2407.2	2.546	5.5
	130	149.7	57.6	2470.3	2.546	4.2
	150	149.9	58.3	2508.9	2.546	4.1
	170	149.7	56.8	2489.1	2.546	2.2
RAP B	110	149.8	57.81	2530.2	2.574	3.5
	130	149.8	58.51	2579.1	2.574	2.8
	150	149.7	56.39	2483.4	2.574	2.8
	170	149.7	57.92	2572.9	2.574	1.9
RAP C	110	149.7	63.3	2705.5	2.565	5.4
	130	149.5	65.2	2818.7	2.565	4.0
	150	149.7	62.0	2651.2	2.565	5.4
	170	149.8	65.2	2789.7	2.565	5.4

Note: G_{mm} is the maximum theoretical relative density of the mix and V_a is air voids.

The V_a (%) was calculated according to Equation 1, based on the apparent volume of the specimen and dry mass.

$$V_a(\%) = \frac{G_{mm} - G_{mb}}{G_{mm}} \times 100 \quad (1)$$

Where: V_a (%) is the air void content in percent, G_{mm} is the theoretical maximum specific gravity; and G_{mb} is the apparent bulk specific gravity.

2.2 Methods

In this study, the LVE properties of the specimens were obtained through IRT, using an analytical method to determine norm of complex modulus ($|E^*|$) and phase angle (φ).

2.2.1 IRT

The IRT consists of recording the vibrational response of a specimen subjected to mechanical excitation, in order to interpret such vibration considering the geometry of such specimen and extract material properties, such as E^*. The natural frequencies, obtained for different modes of vibrations, are directly linked to the intrinsic mechanical properties of the tested material. In this study, the IRT was carried out using a miniature impact hammer equipped with a load cell and a piezoelectric accelerometer, connected to a signal conditioner and a data acquisition system. To reproduce free boundary conditions, the specimens were supported on soft foam. The IRT was performed in two different laboratories, one at a university laboratory and the other at an industry laboratory, to analyze the reproducibility of the proposed methodology. The equipment and main system characteristics used in both laboratories are presented in Table 2.

Table 2. Comparison of equipment and acquisition characteristics between the university and industry laboratories.

	University laboratory	**Industry laboratory**
Impact hammer	model PCB 086E80	model PCB 086E80
Hammer sensitivity (mV/N)	23.29	22.56
Piezoelectric accelerometer	model PCB 353B15	model PCB 353B15
Accelerometer sensitivity (mV/g)	9.70	10.22
Signal conditioner	model PCB 482C15	PCB 480B21
Data acquisition system	NI DAQ USB-6341	NI USB-6210
Sampling frequency	250 000	125 000

Fig. 1 shows the test setup for the flexural mode and the position of the accelerometer and of the impacts for each mode of vibrations. In the symmetric mode, the impacts were applied at the center of the upper surface, while for the antisymmetric mode, the impacts were applied near the edge. The disc geometry was chosen to perform IRT in AM based on previous work from Rezaeizadeh Herozi et al. [25], who investigated the appropriate specimen geometry of AM for quality control purposes using the IRT.

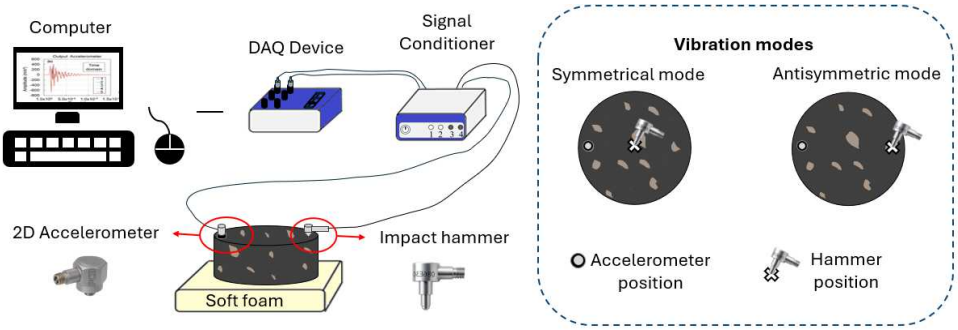


Fig. 1 Setup of the IRT and positions of the sensors for the different modes of vibrations.

The specimens were tested at 5 temperatures (-30, 7, 21.6, and 40 °C), with five impacts applied in each test, to ensure test's repeatability [18, 19, 22-27]. The specimens were conditioned for four hours in a climatic chamber and tested within one minute and thirty-five seconds after removal to measure both vibration modes. The variation of temperature induced by such a small duration is assumed to be negligible.

The signals recorded by the hammer load cell and accelerometer were acquired in the time domain, as shown in Fig. 2 for specimen RAP B, compacted at 150 °C and tested at 21.6 °C in the symmetrical mode. The signals were subsequently transformed into the frequency domain using the fast Fourier transform (FFT), with a 1 Hz frequency resolution. Fig. 3 shows the frequency-domain transforms of the impacts and the corresponding recorded accelerations for the same specimen as in Fig. 2.

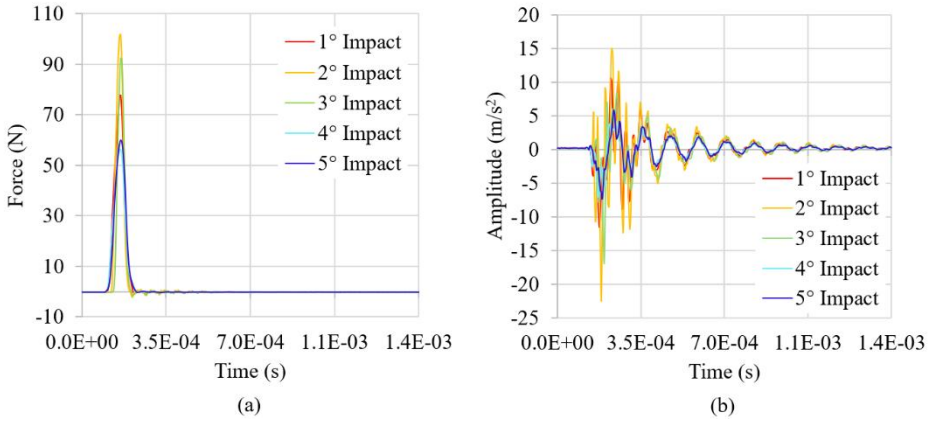


Fig. 2 Experimental data for specimen RAP B, compacted at 150 °C and tested at 21.6 °C in the symmetrical mode: (a) Force (N); and (b) Acceleration amplitude (m/s^2) in time domain.

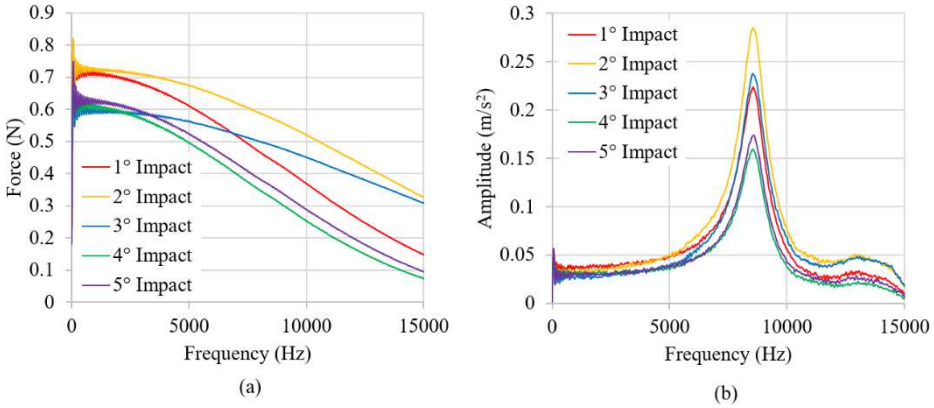


Fig. 3 Experimental data for specimen RAP B, compacted at 150 °C and tested at 21.6 °C in the symmetrical mode:(a) Force (N); and (b) Acceleration amplitude (m/s^2) in frequency domain.

Once the signals were transformed into the frequency domain, the frequency response functions (FRF) were calculated to characterize the system over a wide frequency range. The FRFs were determined as the ratio between the output signal measured by the accelerometer and the input signal generated by the impact hammer. In this study, the FRFs were calculated for each impact, and the average was then obtained from the five repetitions. The average FRF was calculated according to Equation 2. In addition, the coherence function (CF) was calculated according to Equation 3. The CF is a quantitative indicator of reliability, showing how well the output signal matches the input signal at different frequencies. Signals with low

coherence indicate that they may not be a direct result of each other, while good coherence indicates such a relationship. For example, values above 0.9 reflect excellent correlation, with minimal noise or external interference. In contrast, values below 0.8 indicate increased noise, possible problems in the measurement system, or non-linearities.

$$FRF\ (f) = \frac{\overline{Y(f).X^*(f)}}{\overline{X(f).X^*(f)}} \tag{2}$$

$$CF\ (f) = \frac{|\overline{Y(f).X^*(f)}|^2}{|\overline{X(f).X^*(f)}|.|\overline{Y(f).Y^*(f)}|} \tag{3}$$

Where: $FRF\ (f)$ is the frequency response functions, $Y(f)$ is the FFT of the measured acceleration signal, $X(f)$ is the FFT of the applied force signal, $Y^*(f)$ is the complex conjugate of $Y(f)$, $X^*(f)$ is the complex conjugate of $X(f)$, f represents the frequency (the overbars denote the arithmetic mean of the five repetitions) and $CF\ (f)$ is the coherence function.

Fig. 4 shows an example of the average FRF and CF for the RAP B, compacted at 150 °C and tested at 21.6 °C in symmetric mode. It can be seen that in the vicinity of the resonance frequency (about 8.5 kHz), between 5.000 and 10.000 Hz, the CF remains close to 1, indicating high-quality measurements over the displayed frequency range.

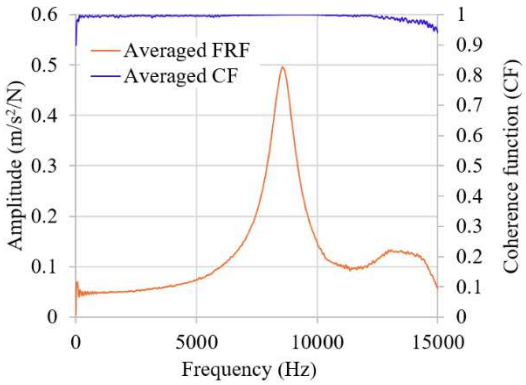


Fig. 4 Experimental data for specimen RAP B, compacted at 150 °C and tested at 21.6 °C in the symmetrical mode: average FRF and CF.

2.2.2 Analytical method for test results' interpretation

For each test, the fundamental resonance frequency, corresponding to the first maximum amplitude of the FRF, was identified. Then, the analytical procedure previously applied to AM by Zhang et al. [28], and initially developed by Martincek [29] for thick circular plates, was used to determine $|E^*|$ from the FRF and φ using the half-power bandwidth method [30]. The modulus of elasticity was calculated according to Equation 4, following Martincek's method [19]:

$$E' = \frac{48\pi^2 f_{nrs}^2 R^4 \rho(1-\nu)}{\mu^2 h^2} \tag{4}$$

where: E' is the modulus of elasticity, f_{nrs} is the undamped resonance frequency corresponding to the first natural frequency of the symmetric mode, R is the radius of the

specimen, ρ is the density of the specimen, ν is Poisson's ratio calculated as a function of h/R and f_{nrs}/f_{nra}, f_{nra} is the first natural frequency of the antisymmetric mode, μ is a coefficient measured by h/R and ν; and h is the thickness of the specimen.

Equation 5 was applied to convert the damped resonance frequencies (f_{dr}) into undamped resonance frequencies (f_{nr}), since the viscous behavior of asphalt mixtures causes the measured resonance frequencies to be damped.

$$f_{nr} = \frac{f_{dr}}{\sqrt{(1-\xi^2)}} \tag{5}$$

Where: f_{nr} is the undamped resonant frequency, f_{dr} is the damped resonant frequency, and ξ is the damping ratio.

As mechanical waves propagate through the specimen, some of the energy is dissipated, leading to a progressive decrease in the amplitude of the vibration. This dissipative behavior is associated with the viscous response of the material and can be represented by the damping ratio. In the present study, this parameter was determined using the half-power bandwidth method. The two frequencies (f_1, f_2) that define the bandwidth were corresponding to 0.707 of the maximum amplitude, as illustrated in Fig. 5. The damping ratio was determined according to Equation 6.

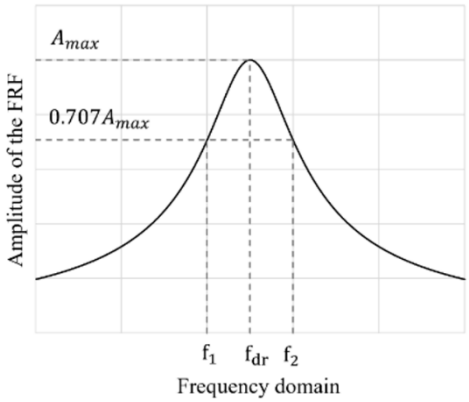


Fig. 5 Damping ratio calculation using the half-power bandwidth method. Adapted from Carret et al. [19].

$$\xi = \frac{f_2 - f_1}{2f_{dr}} \tag{6}$$

Where: $f_{1,2}$ are the half-power frequencies corresponding to an amplitude equal to 0.707 times the maximum amplitude.

The E^* of AM is composed of two components, as shown in Equation 7.

$$E^* = E' + iE'' \tag{7}$$

Where: E^* is complex modulus, E' is elastic modulus, E'' is loss modulus; and i is the imaginary unit.

The magnitude of the complex modulus was calculated according to Equation 8.

$$|E^*| = \frac{E'}{COS\,\varphi} \quad (8)$$

Where, φ represents the phase angle, which was determined from its relationship with the damping ratio according to Equation 9.

$$\varphi = tan^{-1}(2\xi) \quad (9)$$

2.3 Statistical analysis

The reliability of the experimental procedure was evaluated by analyzing repeatability and reproducibility in both university and industrial laboratories. These analyses aim to validate consistency within and across laboratories, providing information on the methodology's potential applicability in both research and industrial contexts.

Repeatability. Test repeatability of the IRT was assessed based on the variability among the five impacts applied in each test. For each individual impact, the norm of complex modulus ($|E^*|$) and phase angle (φ) were determined following the methodology described in Section 2.2.2. The standard deviation (SD) and the coefficient of variation (CV) for $|E^*|$ and φ, calculated from the five individual FRFs. The coherence function (Eq. 3) was also used as a quality criterion for each measurement.

Reproducibility. The reproducibility of the IRT was assessed by comparing the results obtained independently in a university laboratory and an industry laboratory for temperatures of 7, 21.6, and 40 °C. The same specimens were tested in both laboratories. Between the testing campaigns, the specimens were stored in their respective boxes in a laboratory at room temperature. The tests at 40 °C were conducted with approximately a one-year interval between the university and industrial laboratories. The remaining tests at 7 and 21.6 °C were performed with approximately a two-week difference between laboratories. The values of $|E^*|$ and φ, determined from the average FRF of the five impacts, were considered, following the procedure described in Sections 2.2.1 and 2.2.2. In total, 36 pairs of results were compared. The agreement between laboratories was analyzed using: (i) the coefficient of determination (R^2) of the linear relationship between the two sets of measurements; (ii) the difference between laboratories as a function of the mean of the two measurements, expressed in relative terms for $|E^*|$ and in absolute terms for φ; (iii) the bias, defined as the mean difference between laboratories; and (iv) Lin's concordance correlation coefficient (CCC), which evaluates both correlation and deviation from the line of equality:

$$CCC = \frac{2s_{xy}}{s_{x^2} + s_{y^2} + s_{xy}} \quad (10)$$

where $\bar{x}$ and $\bar{y}$ are the means, s_{x^2} and s_{y^2} the variances, and s_{xy} the covariance of the measurements from the two laboratories. These metrics were calculated for the entire dataset and for subgroups defined by test temperature and RAP source.

3 Results

3.1 Repeatability and reproducibility of the IRT

Before using the IRT results to compare and distinguish between the different RAP sources, the reliability of the experimental procedure was first evaluated by analyzing repeatability within each laboratory and reproducibility between the university and industry laboratories.

3.1.1 Repeatability of the IRT

Table 3 presents an example of repeatability analysis for RAP A compacted at 110 °C and tested at 7 °C. An analysis of the data in Table 3 reveals standard deviations of 45.4 MPa for $|E^*|$ and 0.036° for φ, corresponding to coefficients of variation (CV) of 0.198% and 1.0%, respectively. These low values indicate minimal variability among the impacts. Furthermore, the results obtained from the average of the five impacts and from the average FRF were very close, with differences of approximately 0.06% for $|E^*|$ and 0.14% for φ, demonstrating good consistency between the two processing methods.

Table 3. Example of repeatability analysis for RAP A compacted at 110 °C and tested at 7 °C.

Impact	$\|E^*\|$	φ
1	22993.2	3.555
2	22928.7	3.653
3	23056.5	3.609
4	22974.4	3.652
5	22939.5	3.606
Mean	22978.5	3.615
Mean FRF	22992.0	3.610
Standard deviation	45.4	0.036
CV (%)	0.198	1

Fig. 6 shows the mean standard deviation of $|E^*|$ and φ for the tests performed in the university and industry laboratories. The industry laboratory performed tests at temperatures of 7, 21.6 and 40°C. A combined analysis of the results from both laboratories was also performed for these three temperatures. The error bars represent the dispersion of the repeatability values obtained from the different tests considered in each group.

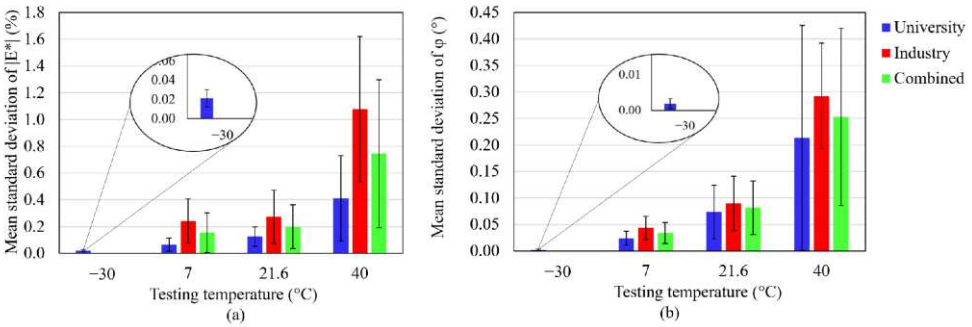


Fig. 6 Mean standard deviation as a function of testing temperature for the university laboratory, industry laboratory, and the combined dataset: (a) Norm of complex modulus, $|E^*|$; and (b) Phase angle, φ.

In general, Fig. 6 shows an increase in result variability as the test temperature rises, for both $|E^*|$ and φ. At university laboratory, the mean standard deviation of $|E^*|$ increased from approximately 0.02% at −30 °C to 0.41% at 40 °C, while that of φ increased from approximately 0.002° to 0.21° over the same temperature range. This trend was also observed at industry laboratory, where the mean standard deviation increased from 0.24% to 1.08% for $|E^*|$ and from 0.04° to 0.29° for φ between 7 and 40 °C. The larger error bars observed at higher temperatures indicate a greater dispersion among the standard deviations calculated for the individual tests. This dispersion can be strongly influenced by isolated tests in which one of the five impacts produced a result that differed more noticeably from the others, resulting in a higher standard deviation for that specific test. Therefore, the larger error bars do not necessarily indicate a general loss of repeatability at higher temperatures, but rather that some individual tests exhibited greater variability among impacts. The greater occurrence of such variability at higher temperatures may be associated with the increasingly viscous response of the material as temperature rises.

At the temperatures where the two laboratories could be compared, the industry laboratory obtained higher mean standard deviation values than those obtained at university laboratory. These differences may be partly inherent to the differences between the equipment and the system's main characteristics, as shown in Table 2. The laboratories used different signal conditioning and data acquisition systems, as well as different sampling frequencies. Despite these differences and the increase in variability with testing temperature, the levels of variability remained low relative to the measured quantities, indicating good repeatability of the IRT procedure in both laboratories.

3.1.2 Reproducibility of the IRT

Fig. 7 presents a direct comparison between the results obtained at university and industry laboratories. For both parameters, a strong linear relationship is observed between the measurements performed at the two laboratories, with an R^2 of approximately 0.96 for $|E^*|$ and 0.95 for φ. This correlation indicates that both capture the same property variations across the tests.

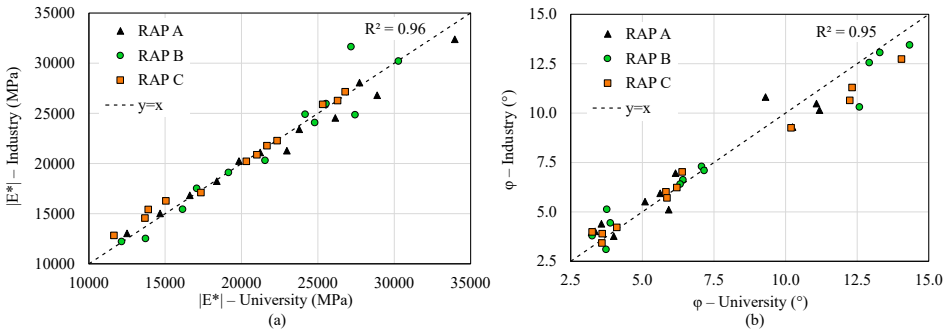


Fig. 7 Agreement between **university and industry** laboratories measurements for (a) Norm of complex modulus, $|E^*|$; and (b) Phase angle, φ.

To deepen the analysis, both parameters were analysed in relation to their mean values. Fig. 8 shows the difference between the parameters $|E^*|$ and φ obtained at the two laboratories as a function of the mean of the corresponding measurements. In Fig. 8a, it can be seen that most (25/36 points) of the relative differences in $|E^*|$ fell within the ±5% range, with nine points lying outside this interval. Regarding φ, the graph in Fig. 8b shows that the differences remained concentrated near zero and within the ±2° range (35/36 points), except for a single value. These results indicate good agreement between the laboratories.

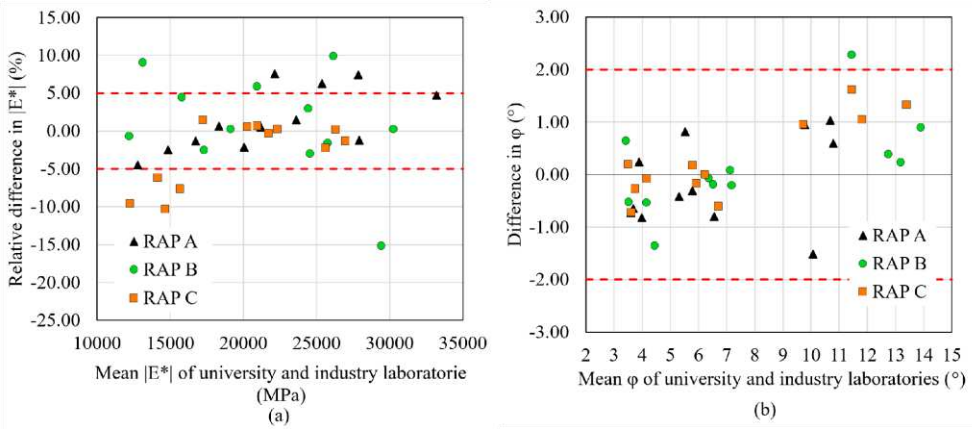


Fig. 8 Differences between **university and industry** laboratories measurements as a function of their mean values for (a) Norm of complex modulus, $|E^*|$; and (b) Phase angle, φ.

To complement the analysis, Table 4 presents metrics for assessing the reproducibility of the evaluated parameters, considering both a general analysis of the data and results grouped by test temperature and RAP source. In the general data analysis, low bias values were observed for both parameters: 46 MPa for $|E^*|$ and 0.08° for φ. The corresponding values for Lin's concordance correlation coefficient (CCC) were 0.977 and 0.968, respectively. As the CCC values are close to 1, they indicate high overall agreement between the two laboratories.

Table 4. Reproducibility metrics for $|E^*|$ and φ between the university and industry laboratories.

Grouping	n	Bias$_{|E^*|}$ (MPa)	CCC$_{|E^*|}$	Bias$_{\varphi}$ (°)	CCC$_{\varphi}$
Overall	36	46	0.977	0.08	0.968
7 °C	12	416	0.838	-0.39	0.100
21.6 °C	12	67	0.988	-0.14	0.77
40 °C	12	-345	0.927	0.76	0.66
RAP A	12	531	0.983	-0.19	0.946
RAP B	12	36	0.962	0.13	0.974
RAP C	12	-429	0.989	0.28	0.973

However, when the results were grouped by testing temperature and RAP source, the bias values for $|E^*|$ were higher than that obtained from the overall dataset, but they are relatively small compared with the magnitude $|E^*|$ (0.11%-4.25%). The CCC values for $|E^*|$ remained close to 1, with the lowest value, 0.838, obtained for the data grouped at 7°C. For φ, lower CCC values were obtained when the analysis was grouped by testing temperature, mainly at 7°C, where CCC decreased to 0.1. This low CCC should be interpreted considering the limited variability of φ within this temperature group. When the measurements are concentrated within a narrow range, relatively small differences between laboratories can substantially reduce the CCC, even when the absolute differences remain small, as indicated by the bias of -0.39°. In contrast, when the data were grouped by RAP source, a broader range of φ values was considered and the CCC values ranged from 0.946 to 0.974. Overall, the bias values for φ remained below 1° in all groups. The time intervals between testing campaigns and potential changes in the specimens during storage may also have contributed to the differences observed between laboratories.

In summary, the analyses confirm that the IRT yields consistent measurements when conducted independently in both laboratories, supporting the reproducibility of the experimental procedure. Therefore, only the results obtained from the university laboratory will be presented in following sections, as that laboratory evaluated the specimens across the entire temperature range considered in this study.

3.2 Effect of compaction temperature and air void content

Fig. 9 presents the $|E^*|$ and φ as a function of compaction temperature for the three RAP groups. The results are shown with different markers, one per the RAP source (triangle, RAP A; circle, RAP B; square, RAP C). The colors of the markers were assigned according to the testing temperatures (blue, −30 °C; green, 7 °C; yellow, 21.6 °C; and red, 40 °C). Fig. 9a indicates that $|E^*|$ increase as the test temperature decreases as expected from the temperature-sensitive nature of asphalt mixtures. $|E^*|$ also tend to increase with compaction temperature rises. These trends are consistently observed across the three RAP materials, despite some isolated variations.

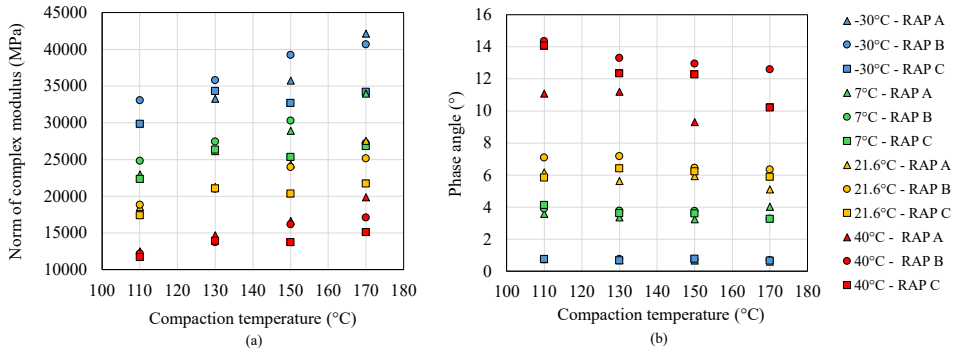


Fig. 9 Effect of compaction temperature on (a) Norm of complex modulus, $|E^*|$, and (b) Phase angle, φ, for RAP A, RAP B, and RAP C.

Fig. 9b shows that the φ increases as the test temperature rises, reflecting an increasing viscous contribution to the viscoelastic response. With respect to compaction temperature, however, φ decreases as it increases. Additional chemical and advanced rheological tests should be performed to better understand this trend.

Fig. 10 presents $|E^*|$ and φ as a function of air void content for the three RAP groups. Fig. 10a shows a general trend of decreasing $|E^*|$ values as air void content increases. This trend is consistently observed across the three RAP materials, despite some scatter. Overall, $|E^*|$ property is affected by both compaction temperature and variations in air void content. In contrast, an analysis of Fig. 10b shows no clear relationship between φ and the air void content; in other words, φ is not directly influenced by the air void content. This is to be expected, given that φ is related to viscous behavior and, consequently, to the rheological characteristics of the bitumen. Hence, φ may serve as a more suitable parameter for comparing the response of different RAP sources, as it minimizes the influence of air void content differences between specimens.

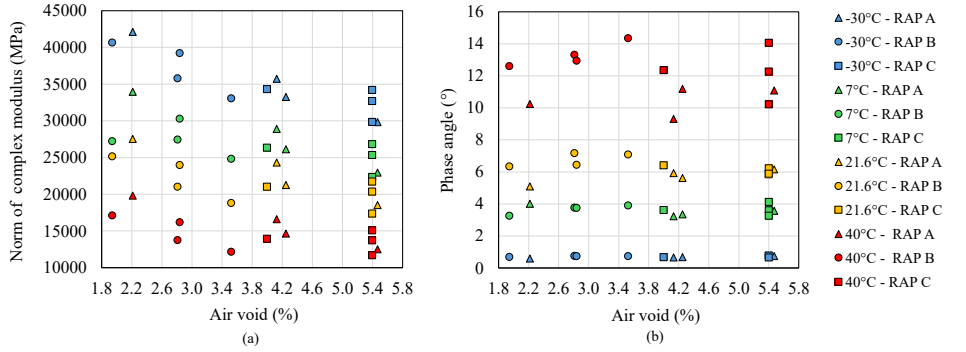


Fig. 10 Relationship between air void content and (a) Norm of complex modulus, $|E^*|$, and (b) Phase angle, φ, for RAP A, RAP B, and RAP C.

3.3 Comparison of RAP source

Because $|E^*|$ depends on both compaction temperature and air void content (Section 3.2), it is difficult to use this parameter in isolation to compare RAP sources. In contrast, no clear relationship was observed between air void content and φ. Two indicators were therefore defined to compare the RAP sources at 40 °C, where the viscous contribution is greater and differences between materials and compaction conditions are more apparent. The first is the ratio $|E^*|_{170}/|E^*|_{110}$ between specimens compacted at 170 °C and 110 °C. The second is the phase angle variation $\Delta\varphi_{170-110} = \varphi_{170} - \varphi_{110}$, where a negative value indicates a decrease in φ with increasing compaction temperature. Fig. 11 presents both indicators.

Fig. 11a shows that RAP A exhibited the highest $|E^*|_{170}/|E^*|_{110}$ ratio at 40°C. (approximately 1.58), followed by RAP B (approx. 1.40) and RAP C (approx. 1.29). However, this ratio must be interpreted with caution because it is influenced by air void content. The exception is RAP C, whose two analyzed samples have the same void content. For RAP A and RAP B, however, the air void content decreased by 3.3 and 1.6 percentage points, respectively, when comparing specimens compacted at 110°C to those compacted at 170°C.

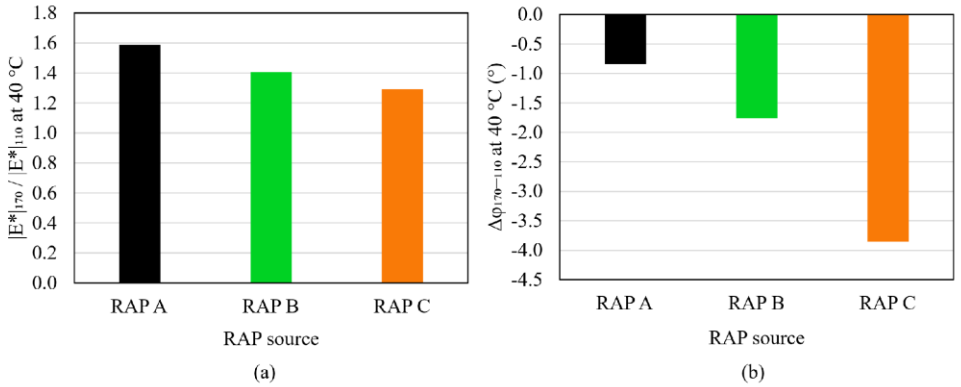


Fig. 11 Effect of compaction temperature on the response of different RAP sources at 40 °C: (a) Norm of complex modulus ratio, $|E^*|_{170}/|E^*|_{110}$; and (b) Phase angle variation, $\Delta\varphi_{170-110}$.

The variation of φ with compaction temperature was taken as the main indicator for comparing the response of the three RAP sources. For this analysis, results obtained at 40°C were used, as φ is sufficiently high under this condition for differences between the RAP sources and compaction conditions to become more apparent. The sensitivity of each material to compaction temperature was quantified as the difference in φ values between specimens compacted at 110°C and 170°C. Fig. 11b shows the variation in $\Delta\varphi_{170-110}$ at 40°C. RAP A exhibited the smallest variation (in magnitude) of approximately -0.8°, followed by RAP B and RAP C approximately -1.8° and -3.9°, respectively.

These results indicate that the three RAP sources exhibited different variations in φ response to increasing compaction temperature, with the magnitude of $\Delta\varphi$ progressively increase from RAP A to RAP C. Therefore, under the conditions investigated in this study, $\Delta\varphi$ may be a useful indicator for differentiating between RAP sources to compaction temperature. However, these results should be interpreted considering the experimental program's limitations, as only one specimen was analysed for each compaction temperature and RAP source, and air void content was not controlled.

4 Conclusion

This study proposes a methodology based on the Impact Resonance Test (IRT) for the non-destructive characterization of the viscoelastic response and differentiation of 100% RAP sources. The methodology was applied to three RAP sources, leading to the following conclusions:

- IRT demonstrated good repeatability in both the university and industry laboratories, with low variability among the five impacts performed in each test. Furthermore, comparing results obtained in the two laboratories showed good overall reproducibility in determining $|E^*|$ and φ. These findings support the reliability and consistency of the proposed methodology and highlight its potential applicability in both academic research and industrial practice.
- Applying the IRT at different test temperatures allowed for the characterization of the viscoelastic response of RAP sources, identifying variations in $|E^*|$ and φ associated with different compaction temperatures and air void content.
- Analysis showed that $|E^*|$ is influenced by both compaction temperature and air void content. Conversely, no clear relationship was observed between φ and void content under the conditions studied. The analysis of $\Delta\varphi$ between specimens compacted at 110°C and 170°C for the three RAP sources, based on results obtained at 40°C, indicated the parameter's potential to differentiate RAP sources according to their response to compaction temperature.

Overall, the results demonstrate the methodology's potential to characterize and distinguish the viscoelastic response of 100% RAP from different sources without requiring binder extraction. However, at this stage of the study, only one specimen was produced for each compaction temperature and RAP source, and air void content was not controlled. Future work should apply the methodology to a larger number of specimens and RAP sources while controlling air void content at the various compaction temperatures, thereby allowing for a more in-depth analysis of the methodology's potential to differentiate between RAP sources.

References

1. Milad, A., Taib, A. M., Ahmeda, A. G., Solla, M., & Yusoff, N. I. M. (2020). A review of the use of reclaimed asphalt pavement for road paving applications. *J. Teknol*, *82*(3), 35-44. https://doi.org/10.11113/jt.v82.14320
2. Tsakoumaki, M., & Plati, C. (2024). A critical overview of using reclaimed asphalt pavement (RAP) in road pavement construction. *Infrastructures*, *9*(8), 128. https://doi.org/10.3390/infrastructures9080128
3. Mariyappan, R., Palammal, J. S., & Balu, S. (2023). Sustainable use of reclaimed asphalt pavement (RAP) in pavement applications—a review. *Environmental Science and Pollution Research*, *30*(16), 45587-45606. https://doi.org/10.1007/s11356-023-25847-3
4. Abdel-Jaber, M. T., Al-shamayleh, R. A., Ibrahim, R., Alkhrissat, T., & Alqatamin, A. (2022). Mechanical properties evaluation of asphalt mixtures with variable contents of reclaimed asphalt pavement (RAP). *Results in Engineering*, *14*, 100463. https://doi.org/10.1016/j.rineng.2022.100463
5. Bilema, M., Aman, M. Y., Hassan, N. A., Memon, Z. A., Omar, H. A., Yusoff, N. I. M., & Milad, A. (2021). Mechanical performance of reclaimed asphalt pavement modified with waste frying oil and crumb rubber. *Materials*, *14*(11), 2781. https://doi.org/10.3390/ma14112781

6. Sadeghi, P., Karimi, A., Torbatifard, S., & Goli, A. (2024). A comprehensive evaluation of damping, vibration, and dynamic modulus in reclaimed asphalt pavement: The role of rejuvenators, polymer, temperature, and aging. *Case Studies in Construction Materials*, *21*, e03366. https://doi.org/10.1016/j.cscm.2024.e03366
7. Imaninasab, R., Loria-Salazar, L., & Carter, A. (2023). Linear viscoelastic behavior of asphalt binders and mixtures containing very high percentages of reclaimed asphalt pavement. *Frontiers of Structural and Civil Engineering*, *17*(8), 1211-1227. https://doi.org/10.1007/s11709-023-0983-9
8. Orosa, P., Orozco, G., Carret, J. C., Carter, A., Pérez, I., & Pasandín, A. R. (2022). Compactability and mechanical properties of cold recycled mixes prepared with different nominal maximum sizes of RAP. *Construction and Building Materials*, *339*, 127689. https://doi.org/10.1016/j.conbuildmat.2022.127689
9. Raschia, S., Moghaddam, T. B., Perraton, D., Baaj, H., Carter, A., & Graziani, A. (2021). Effect of rap source on compactability and behavior of cold-recycled mixtures in the small strain domain. *Journal of Materials in Civil Engineering*, *33*(4), 04021030. https://doi.org/10.1061/(ASCE)MT.1943-5533.0003614
10. Raschia, S., Graziani, A., Carter, A., & Perraton, D. (2019). Laboratory mechanical characterisation of cold recycled mixtures produced with different RAP sources. *Road Materials and Pavement Design*, *20*(sup1), S233-S246. https://doi.org/10.1080/14680629.2019.1588775
11. Bérubé, M. A., Lamothe, S., Bilodeau, K., & Carter, A. (2025). Exploring the effects of reclaimed asphalt pavement on hot-mix asphalt performance and the use of blending charts to predict them: A laboratory investigation. *Journal of Testing and Evaluation*, *53*(2), 349-364. https://doi.org/10.1520/JTE20240236
12. Song, Y., Xu, H., Wu, S., Xie, J., Chen, A., Lv, Y., ... & Li, Y. (2024). High-quality utilization of reclaimed asphalt pavement (RAP) in asphalt mixture with the enhancement of steel slag and epoxy asphalt. *Construction and Building Materials*, *445*, 137963. https://doi.org/10.1016/j.conbuildmat.2024.137963
13. Colbert, B., & You, Z. (2012). The determination of mechanical performance of laboratory produced hot mix asphalt mixtures using controlled RAP and virgin aggregate size fractions. *Construction and Building Materials*, *26*(1), 655-662. https://doi.org/10.1016/j.conbuildmat.2011.06.068
14. Ma, J., Dean, G., Nawarathna, H. M., & Hesp, S. A. (2023). Development and validation of an accurate, precise and safe method for the acceptance testing of recovered asphalt binder. *Construction and Building Materials*, *409*, 133960. https://doi.org/10.1016/j.conbuildmat.2023.133960
15. Zhong, H., Huang, W., Lin, P., Zhou, L., & Lv, Q. (2023). Critical considerations and effective assessment of extraction and recovery processes of RAP. *Construction and Building Materials*, *403*, 133039. https://doi.org/10.1016/j.conbuildmat.2023.133039
16. Carret, J. C., & Babadopulos, L. (2025). Opening Letter of RILEM TC MWP: Mechanical wave propagation to characterize bituminous mixtures. *RILEM Technical Letters*, *10*:15-21. https://doi.org/10.21809/rilemtechlett.2025.211
17. Gudmarsson, A., Ryden, N., Di Benedetto, H., & Sauzéat, C. (2015). Complex modulus and complex Poisson's ratio from cyclic and dynamic modal testing of asphalt concrete. *Construction and Building Materials*, *88*:20-31. https://doi.org/10.1016/j.conbuildmat.2015.04.007
18. Carret, J. C., Di Benedetto, H., & Sauzéat, C. (2018). Characterization of asphalt mixes behaviour from dynamic tests and comparison with conventional cyclic tension–compression tests. *Applied Sciences*, *8*(11), 2117. https://doi.org/10.3390/app8112117
19. Carret, J. C., Bilodeau, K., Herozi, M. R., & Babadopulos, L. (2025). Effects of air void content and back-calculation techniques on bituminous mixture modulus via impact resonance. *Materials and Structures*, *58*(6), 224. https://doi.org/10.1617/s11527-025-02734-6

20. Mounier, D., Di Benedetto, H., & Sauzéat, C. (2012). Determination of bituminous mixtures linear properties using ultrasonic wave propagation. *Construction and Building Materials*, *36*, 638-647. https://doi.org/10.1016/j.conbuildmat.2012.04.136
21. LaCroix, A., Kim, Y. R., Sadat, M., & Far, S. (2009). Constructing the dynamic modulus mastercurve using impact resonance testing. *Journal of the Association of Asphalt Paving Technologists*, *78*.
22. Carret, J. C., Di Benedetto, H., & Sauzeat, C. (2020). Linear viscoelastic behavior of asphalt mixes from dynamic frequency response functions. *International Journal for Numerical and Analytical Methods in Geomechanics*, *44*(7), 1019-1031. https://doi.org/10.1002/nag.3045
23. Gudmarsson, A., Ryden, N., & Birgisson, B. (2014). Observed deviations from isotropic linear viscoelastic behavior of asphalt concrete through modal testing. Construction and Building Materials, 66, 63-71. https://doi.org/10.1016/j.conbuildmat.2014.05.077
24. Gudmarsson, A., Ryden, N., Di Benedetto, H., Sauzéat, C., Tapsoba, N., & Birgisson, B. (2014). Comparing linear viscoelastic properties of asphalt concrete measured by laboratory seismic and tension–compression tests. Journal of nondestructive evaluation, 33(4), 571-582. https://doi.org/10.1007/s10921-014-0253-9
25. Rezaeizadeh Herozi, M., Carret, J. C., Babadopulos, L. F., & Bilodeau, K. (2025). Numerical and experimental investigation of the appropriate geometry of asphalt specimens for quality control using impact resonance tests. Journal of Testing and Evaluation, 53(5), 1251-1268. https://doi.org/10.1520/JTE20240298
26. Carret, J. C., Di Benedetto, H., & Sauzéat, C. (2018). Back analysis of impact loadings on viscoelastic specimen. Paper presentation, 10th International Conference on Road and Airfield Pavement Technology (ICPT 2017), Hong Kong, China, August 8–10, 2017.
27. Carret, J. C., Pedraza, A., Di Benedetto, H., & Sauzeat, C. (2018). Comparison of the 3-dim linear viscoelastic behavior of asphalt mixes determined with tension-compression and dynamic tests. *Construction and Building materials*, *174*, 529-536. https://doi.org/10.1016/j.conbuildmat.2018.04.156
28. Zhang, L., Li, T. S., & Tan, Y. Q. (2016). The potential of using impact resonance test method evaluating the anti-freeze-thaw performance of asphalt mixture. *Construction and Building Materials*, 115, 54-61.https://doi.org/10.1016/j.conbuildmat.2016.04.026
29. Martinček, G. (1965). The determination of Poisson's ratio and the dynamic modulus of elasticity from the frequencies of natural vibration in thick circular plates. *Journal of Sound and Vibration*, 2(2), 116-127. https://doi.org/10.1016/0022-460X(65)90089-1
30. Bachmann, H. (1991). Vibration problems in structures (Vol. 209). *Wien: Bulletin d'information*.